Applied Catalysis B: Environment and Energy 365 (2025) 124877

Contents lists available at ScienceDirect

Applied Catalysis B: Environment and Energy

journal homepage: www.elsevier.com/locate/apcatb

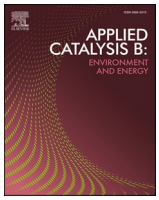

Flattened Pt clusters constructed on CeO_2 for efficient selective oxidation of NH_3

Qinglong Liu [a], Jiawei Yang [a], Shaoxiong Zhang [a], Song Hong [c], Hengxiang Zhang [d], Lupeng Han [d], Dengsong Zhang [d], Fei Gao [b,*], Wei Tan [a,*], Lin Dong [a]

[a] State Key Laboratory of Pollution Control and Resource Reuse, School of Environment, Jiangsu Key Laboratory of Vehicle Emissions Control, Center of Modern Analysis, Key Laboratory of Mesoscopic Chemistry of MOE, School of Chemistry and Chemical Engineering, Nanjing University, Nanjing 210023, China
[b] School of Environmental Science and Engineering, Nanjing University of Information Science and Technology, Nanjing 210044, China
[c] College of Materials Science and Engineering, Beijing University of Chemical Technology, Beijing 100029, China
[d] Innovation Institute of Carbon Neutrality, International Joint Laboratory of Catalytic Chemistry, College of Sciences, Shanghai University, Shanghai 200444, China

ARTICLE INFO

Keywords:
NH_3 oxidation
Pt-CeO_2 interaction
Pt cluster catalysts
Flattened Pt clusters

ABSTRACT

In the field of environmental catalysis, the effective elimination of pollutants with limited generation of harmful byproducts is a general requirement for environmental pollutant elimination catalysts. Recently, the efficient selective catalytic oxidation of NH_3 (NH_3-SCO) with high N_2 selectivity has become a research hotspot. In this work, based on the understanding of the structure-activity relationship for Pt/CeO_2 catalysts in NH_3-SCO reaction, a novel flattened Pt cluster catalyst supported on CeO_2 (FC-Pt/CeO_2) was synthesized by the solution combustion method. In comparison to CeO_2-supported bulky (three-dimensional) Pt cluster/particle catalyst prepared by the conventional incipient wetness impregnation method, flattened Pt clusters with more Pt-O-Ce structure could better facilitate the activation of adsorbed NH_3 at low temperatures, thus achieving superior low temperature NH_3 oxidation activity. It was also revealed that the NH_3-SCO reaction on FC-Pt/CeO_2 was proceeded by *i*-SCR pathway, in which NO generated by the deep oxidation of NH_3 would react with adsorbed NH_3 or -NH_2/-NH. This work provided new insights into constructing robust cluster catalysts from an aspect of cluster shape control, which would significantly benefit the environmental catalysis community.

1. Introduction

Ammonia (NH_3) is a hazardous air pollutant that not only causes damage to the human eyes, skin, and respiratory system, but also significantly contributes to the formation of secondary inorganic aerosols and environmental issues such as eutrophication and particulate matter formation [1–3]. In recent decades, NH_3 has been widely used as a reductant in the selective catalytic reduction (SCR) of nitrogen oxides (NO_x) emitted by both stationary and mobile sources [4–7]. The Ammonia Slip Catalyst (ASC) located at the end of the SCR reactor, is designed for the selective catalytic oxidation of NH_3 (NH_3-SCO) slipping from NH_3-SCR systems, thereby mitigating potential harm to the environment [8,9]. Since the ASC is positioned at the end of after-treatment systems, the exhaust gas temperature in this location is typically low. It often ranges from 200 to 400 °C. Therefore, developing efficient NH_3 oxidation catalysts with superior low-temperature activity is crucial. At same time, achieving satisfactory N_2 selectivity under these conditions has become a major focus in NH_3-SCO research.

Cerium dioxide (CeO_2) has been extensively used in environment and energy-related reactions due to its superior redox performance [10–12]. Besides, the overlap of 4 f and 5d orbitals of Ce atoms not only enabled the facile redox cycle between Ce^{3+} and Ce^{4+} (*i.e.*, electron gain or loss on Ce ions) but also induced the formation of strong interaction between CeO_2 and supported catalytic reactive species, especially platinum group metals (PGMs) [13–17]. Recently, there has been growing interest in increasing the intrinsic reactivity of Pt catalysts supported on CeO_2 through tuning Pt dispersion and the Pt-CeO_2 interaction (or coordination environment of Pt), which have been proven to be effective [18–21].The overly strong Pt-O-Ce interactions can lead to difficulties in reactant desorption, thus resulting in a “self-poisoning” effect [22–24]. As a result, the application of Pt SACs supported on CeO_2 in the environmental catalysis field is still limited comparing to Pt cluster/particle catalysts [25]. Recently, Ge *et al.* and Laís Reis Borges *et al.* demonstrated that the size and morphology of Pt particles influence the density

* Corresponding authors.
E-mail addresses: fgao@nuist.edu.cn (F. Gao), tanwei@nju.edu.cn (W. Tan).

https://doi.org/10.1016/j.apcatb.2024.124877
Received 9 October 2024; Received in revised form 20 November 2024; Accepted 26 November 2024
Available online 27 November 2024

of surface oxygen and the density of Pt-O-Ce sites, which are critical for the catalytic process [26,27].

For NH_3-SCO reaction, the importance of Pt^0 species within Pt cluster/particle and Pt single atoms with a high coordination number of Pt-O-Ce was highlighted in different works [28–32], which inspired us to construct Pt cluster catalysts with unique shapes and proper Pt-O-Ce interaction. Such well-regulated clusters might exhibit superior catalytic performance in NH_3 oxidation reactions. In this work, based on a solution combustion method that has been applied for synthesizing highly dispersed noble metal catalysts [33–35], a novel Pt/CeO_2 catalyst with flattened Pt clusters [36,37] was fabricated. The solution combustion method is inherently scalable due to its reliance on simple precursors and a self-sustained combustion process, which ensures high energy efficiency and low production costs [38]. Comparing to bulky Pt cluster catalyst and atomically dispersion (AD) Pt catalyst prepared by conventional incipient wetness impregnation method, the flattened Pt cluster catalyst with exhibited superior low temperature NH_3 oxidation activity and N_2 selectivity. Systematic characterizations were also conducted to investigate the reaction mechanism and detailed relationship between the catalytic performance and catalyst structure. This work will take the research on efficient NH_3-SCO catalysts a step forward in terms of catalyst preparation and reaction mechanism.

2. Materials and experimental methods

CeO_2 supported flattened Pt clusters (FC-Pt/CeO_2), bulky Pt clusters (BC-Pt/CeO_2) and atomically dispersed Pt (AD-Pt/CeO_2) were prepared by different methods as described below.

FC-Pt/CeO_2 was synthesized by solution combustion method using $(NH_4)_2Ce(NO_3)_6$ and $Pt(NO_3)_2$ as precursors, using dihydrazine oxalate as fluxing agent. $(NH_4)_2Ce(NO_3)_6$ and $Pt(NO_3)_2$ were first dissolved in deionized water in a specified ratio to achieve a platinum loading of 1 at %. Dihydrazine oxalate was then added to the solution under vigorous stirring. The mixture was then transferred to a corundum crucible and placed in a muffle furnace preheated to 400 °C. After vigorous combustion, the furnace door was opened to allow the crucible to cool to room temperature in a short period time. The resulting solid was then ground to a powder.

BC-Pt/CeO_2 with a same Pt loading of 1 at% was synthesized by incipient wetness impregnation (IWI) method, using $Pt(NO_3)_2$ as Pt precursor and CeO_2 prepared by similar solution combustion approach as support. Specifically, $Pt(NO_3)_2$ aqueous solution was meticulously added to CeO_2 support dropwise under vigorous stirring, and then the obtained mixture was then dried at 120 °C for 1 h, followed by calcination at 400 °C in air for 4 h, with a ramping rate of 2 °C/min.

AD-Pt/CeO_2 with a Pt loading of 1 at% was prepared by IWI method, using CeO_2 obtained by thermo-decomposition of $Ce(NO_3)\bullet 6\ H_2O$ at 550 °C as support and $Pt(NO_3)_2$ as Pt precursor. After impregnation, the mixture was calcined at 550 °C in air for 4 h (Pt/CeO_2-550). Besides, to minimize the difference in the specific surface area between those prepared Pt/CeO_2 catalysts, Pt/CeO_2-550 was further calcined at 1000 °C for 2 h to achieve a comparable specific surface area to that of FC-Pt/CeO_2 and BC-Pt/CeO_2.

Furthermore, to investigate the migration of platinum from the bulk phase of CeO_2 to the surface during calcination, a reference Pt/CeO_2 catalyst was also prepared by co-precipitation method. Specifically, $(NH_4)_2Ce(NO_3)_6$ and $Pt(NO_3)_2$ were first dissolved in deionized water under vigorous stirring, and then ammonium hydroxide ($NH_3\bullet H_2O$) was added to the solution until pH reached 10. Afterwards, the mixture was aged overnight, filtered, and washed repeatedly with deionized water until the supernatant was neutral. The obtained gel was subsequently dried at 120 °C for 1 h and calcined in air at 1000 °C for 4 h. The catalyst prepared above was denoted as PtCe-CP-1000. Pt catalyst supported on commercial Al_2O_3 catalysts (Pt/Al_2O_3-C) was also prepared by IWI method as an important reference. $Pt(NO_3)_2$ was used as Pt precursor and the calcination temperature was 550 °C (4 h in air).

Prior to evaluation of catalytic performance, all catalysts were ground, pressed and sieved to 40–60 mesh.

Detailed information of characterizations and catalytic performance evaluation can be found in Supporting Information (Texts S1 and S2).

For experimental data related to AD-Pt/CeO_2, please refer to Figures S4-S7 and Figure S12 in the Supplementary Material.

3. Results and discussion

3.1. Crystal structure and textural properties

X-ray diffraction (XRD) analysis was conducted to characterize the crystalline structure of the prepared Pt/CeO_2 catalysts. As illustrated in Fig. 1a, all Pt/CeO_2 catalysts exhibited the distinctive cubic fluorite structure of CeO_2 (JCPDS#43–1002) [39]. It is noteworthy that no discernible XRD peak assigned to crystalline Pt or PtO_x was observed on FC-Pt/CeO_2, BC-Pt/CeO_2 and AD-Pt/CeO_2, suggesting the high dispersion of Pt species. In contrast, the notable XRD peak at *ca.* 41° indicated that Pt would preferentially migrate to the surface of CeO_2 during the calcination process and crystalline Pt species were formed on PtCe-CP-1000 sample (Figure S1). In other words, the solution combustion method could better facilitate the dispersion of Pt on CeO_2 comparing to co-precipitation method, although the precursors of Pt and Ce were pre-mixed in both two methods. Interestingly, the similar type IV isotherms with H1 hysteresis loops for N_2 adsorption-desorption (Fig. 1b) as well as the comparable specific BET surface areas, pore volumes, average pore sizes (Table 1), which should be due to the well-controlled calcination temperature. Moreover, as listed in Table 1, the real content of Pt (0.72–0.85 wt%) in those prepared Pt/CeO_2 catalysts calculated according to the results of ICP was close to the theoretical Pt content (1.0 wt%). That is, the differences between various Pt/CeO_2 catalysts, if any, should be mainly in terms of Pt states (*e.g.*, dispersion, valence and Pt-CeO_2 interaction).

To investigate the dispersion of Pt, the surface concentration of Pt on Pt/CeO_2 catalysts was first calculated according to the results of XPS (Table 1). It was found that the surface concentration of Pt followed an order of AD-Pt/CeO_2 > FC-Pt/CeO_2 > BC-Pt/CeO_2, indicating that the dispersion of Pt on AD-Pt/CeO_2, FC-Pt/CeO_2 and BC-Pt/CeO_2 was indeed different, as expected when designing the synthesis routes.

AC-HAADF-STEM images and corresponding EDS-mapping images for FC-Pt/CeO_2, BC-Pt/CeO_2 and AD-Pt/CeO_2 were collected to visualize the dispersion of Pt states. As shown in Fig. 2 and Figure S2, Pt clusters were formed on FC-Pt/CeO_2 and BC-Pt/CeO_2, while Pt species on AD-Pt/CeO_2 were atomically dispersed. Moreover, aggregated Pt species on FC-Pt/CeO_2 and BC-Pt/CeO_2 could also be clearly observed in their EDS-mapping images, and Pt species were atomically dispersed on AD-Pt/CeO_2. Interestingly, although Pt species on both FC-Pt/CeO_2 and BC-Pt/CeO_2 were in the form of clusters, Pt clusters on FC-Pt/CeO_2 were more dispersed and showed a flattened configuration (1–2 atom layers), in comparison to those on BC-Pt/CeO_2 with a three-dimensional morphology. Furthermore, according to the results of particle size statistics (Figure S3a-b), the average particle size of Pt clusters on FC-Pt/CeO_2 (1.6 ± 0.6 nm) was slightly smaller than those on BC-Pt/CeO_2 (2.1 ± 0.7 nm).

To further characterize the dispersion state of Pt species, *in situ* DRIFTS analysis of CO adsorption was performed at 30 °C (Fig. 2d-f). For AD-Pt/CeO_2, a distinct symmetrical peak was observed at around 2089 cm^{-1}, indicative of CO adsorbed on ionic Pt atoms (CO-$Pt^{\delta+}$), suggesting that the Pt is predominantly in single atom form [40–42], confirming the AC-HAADF-STEM observations. In contrast, besides the CO-$Pt^{\delta+}$ peak, a weaker band around 2046 cm^{-1} attributed to CO adsorbed on Pt clusters/nanoparticles was also observed on FC-Pt/CeO_2 and BC-Pt/CeO_2 [43–45], confirming the aggregation of Pt species.

With detailed crystal structure and textural properties of Pt/CeO_2 catalysts identified, it is imperative to investigate how these characteristics influence the interactions at the Pt-CeO_2 interface. The following

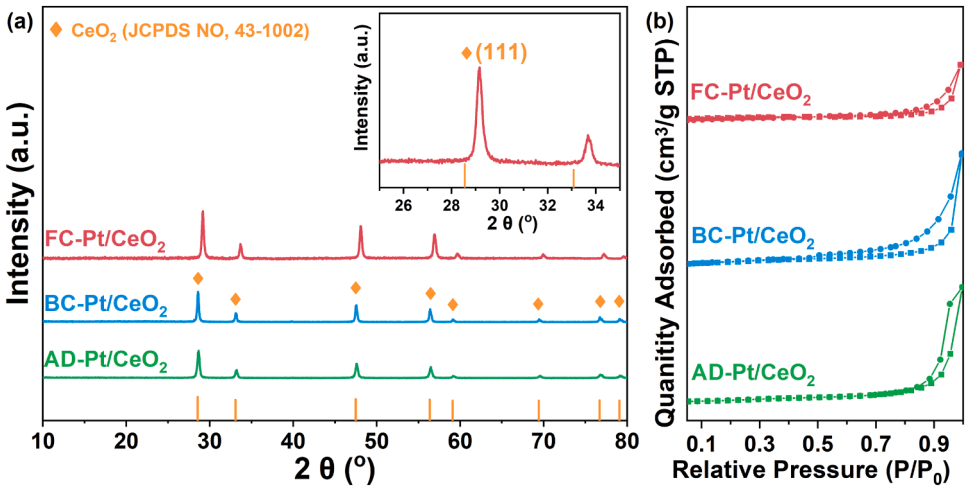

Fig. 1. XRD patterns for a) FC-Pt/CeO_2, BC-Pt/CeO_2 and AD-Pt/CeO_2 catalysts. b) N_2 adsorption-desorption isotherm diagram for FC-Pt/CeO_2, BC-Pt/CeO_2 and AD-Pt/ CeO_2 catalysts.

Table 1
BET surface area and pore volume for Pt/CeO_2 catalysts, Pt loadings determined by ICP and surface atomic concentration determined by XPS.

Samples	BET area (m^2/g)	Pore volume (cm^3/g)	Pore size (nm)	Pt loadings (wt%)	Surface atomic concentration (%)		
					Ce	Pt	O
FC-Pt/CeO_2	8.69	0.03	16.0	0.72	22.6	0.6	76.8
BC-Pt/CeO_2	11.69	0.07	22.7	0.82	21.8	0.5	77.6
AD-Pt/CeO_2	10.92	0.08	20.6	0.85	21.3	0.8	77.9

section delves into the Pt-CeO_2 interactions and the resultant effects on the catalyst surface states, which are critical for understanding the catalytic behavior and reaction mechanisms.

3.2. *Pt-CeO_2 interaction and catalyst surface states*

Raman spectroscopy was used to study the interaction between Pt and CeO_2 in different Pt/CeO_2 catalysts [46]. As shown in Fig. 3a, the peak assigned to the F_{2g} mode of fluorite-type CeO_2 on FC-Pt/CeO_2 showed a redshift from 457 to 447 cm^{-1} and significant peak broadening. These changes are attributed to the doping of Pt ions into the CeO_2 lattice [47]. In addition, two new broad peaks were observed around 570 and 665 cm^{-1} corresponding to bridging Pt-O-Ce vibrations and Pt-O vibrations within the Pt-O-Ce structure, respectively [21]. Notably, the intensity of these two peaks on FC-Pt/CeO_2 was significantly higher than BC-Pt/CeO_2, suggesting the increased exposure of interfacial sites on fully exposed cluster sites. Besides, the more intensive Pt-O and Pt-O-Ce peaks on AD-Pt/CeO_2 should be related to the atomically dispersed Pt on CeO_2 support (Figure S4).

The interaction strength between Pt and CeO_2 was assessed using CO-TPR (Fig. 3b and Figure S5). The CO-consumption peak corresponding to the reduction of Pt-O/Pt-O-Ce appears at higher temperatures for FC-Pt/CeO_2 (94.5 °C) compared to BC-Pt/CeO_2 (85.8 °C), suggesting a stronger Pt-CeO_2 interaction in FC-Pt/CeO_2 [21]. The strong interaction between Pt and CeO_2 could be one of the main reasons for the generation of flattened clusters on FC-Pt/CeO_2. Furthermore, the doping of Pt ions into the CeO_2 lattice has resulted in numerous defect sites on the FC-Pt/CeO_2 surface, as deduced from Raman spectroscopy. The peak at 1174 cm^{-1}, identified as the 2LO vibrational peak of CeO_2, correlates positively with the concentration of oxygen defects [48]. Increased intensity of the Ov-2LO band on FC-Pt/CeO_2 indicates the formation of more oxygen defects. As a complementary, EPR spectroscopy experiment was also performed. A much more intensive signal at g = 2.002, which is typically associated with defect-localized electrons minimally affected by the lattice field, was observed on FC-Pt/CeO_2, further confirming the formation of more defects on FC-Pt/CeO_2 [45]. In addition, the analysis of Ce 3*d* XPS (Fig. 3e) revealed that the surface concentration of Ce^{3+} on the FC-Pt/CeO_2 (35.7 %) is higher than that on DC-Pt/CeO_2 (32.4 %). Considering that the formation of Ce^{3+} was always related to the oxygen vacancies, it could be concluded that more Ce^{3+}-Ov sites were formed on FC-Pt/CeO_2, which possesses smaller flattened Pt clusters. Generally, it is assumed that oxygen vacancies would facilitate the adsorption and activation of oxygen. However, the results of O 1 *s* XPS (Fig. 3f) revealed the ratios of surface adsorbed oxygen species (O_H) to lattice oxygen species (O_L) for FC-Pt/CeO_2 and BC-Pt/CeO_2 were almost the same, suggesting that FC-Pt/CeO_2 may have comparable O_2 adsorption and activation capacities to BC-Pt/CeO_2, well supported by the results of O_2-TPD (Figure S6 and Table S1) that FC-Pt/CeO_2 and BC-Pt/CeO_2 showed similar O_2 desorption characteristics.

The chemical states of Pt species were further elucidated by Pt 4 f XPS (Fig. 4a and Figure S7). It was revealed that Pt species on FC-Pt/CeO_2 and BC-Pt/CeO_2 were in different valence states. In particular, the fraction of surface Pt^0 on FC-Pt/CeO_2 was only 9.6 %, much lower than that on BC-Pt/CeO_2 (28.1 %). The relatively higher oxidation states of Pt species on FC-Pt/CeO_2 should be related to the smaller Pt cluster size, flattened shape, stronger Pt-CeO_2 interaction and more Pt-CeO_2 interfacial sites. To further disclose the electronic and coordination environments of Pt clusters on Pt/CeO_2 catalysts, synchrotron-based X-ray absorption spectroscopy (XAS) was employed, and the extended X-ray absorption fine structure (EXAFS) and X-ray absorption near edge structure (XANES) regions (Fig. 4b-d) were analyzed in detail. Besides using Pt foils and PtO_2 as references, AD-Pt/CeO_2 was also investigated to help identify the dispersion states and coordination environment of Pt species on various Pt/CeO_2 catalysts. The white line intensity of Pt-L_3 XANES for Pt/CeO_2 catalysts, Pt foils and PtO_2 followed an order of PtO_2 > AD-Pt/CeO_2 > FC-Pt/CeO_2 > BC-Pt/CeO_2 > Pt foil, indicating that Pt species on the prepared Pt/CeO_2 catalysts were in oxidation states, and FC-Pt/CeO_2 showed higher average valence than BC-Pt/CeO_2, which was further confirmed by the results of linear combination fitting analysis that the average valence of AD-Pt/CeO_2, FC-Pt/CeO_2 and BC-Pt/CeO_2 was 2.14 ± 0.11, 0.93 ± 0.16 and 0.68 ± 0.24, respectively (Table S2). Moreover, the higher oxidation state of Pt on FC-Pt/CeO_2 comparing to BC-Pt/CeO_2 is well consistent with XPS results.

To reveal the coordination environment of Pt species within the

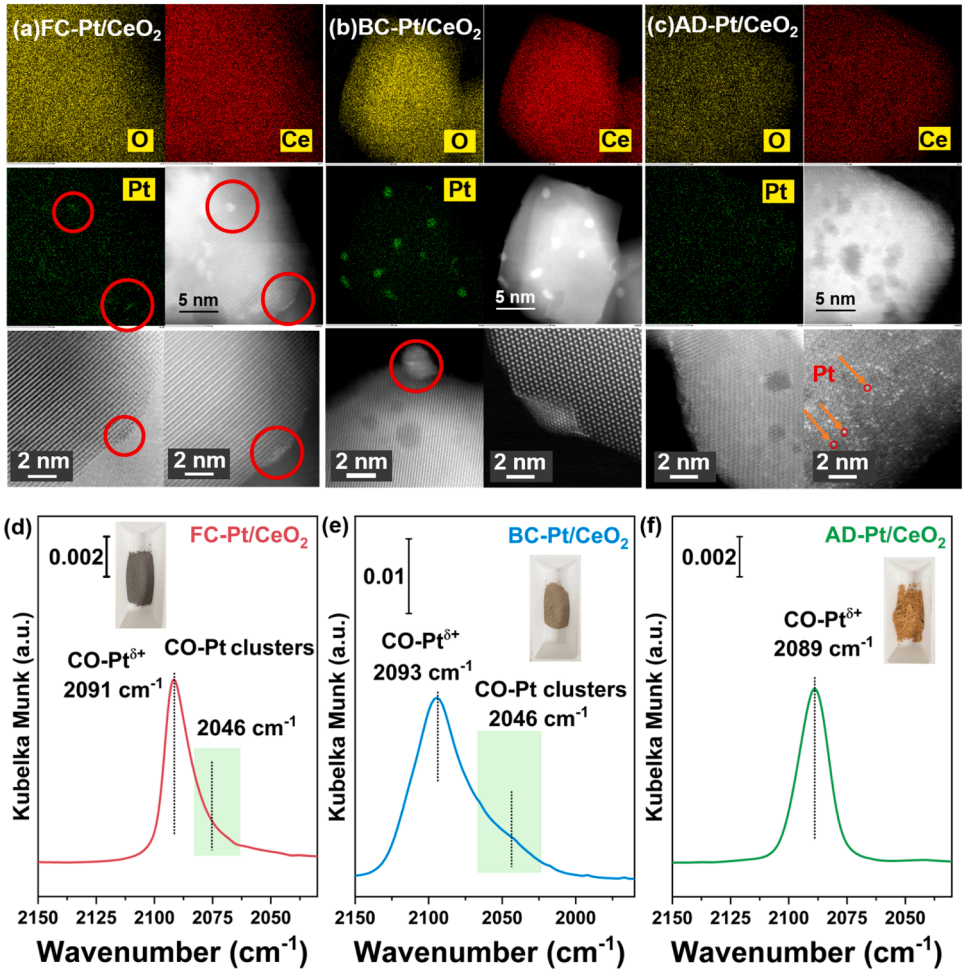

Fig. 2. EDS mapping images and AC-HAADF-STEM images of a) FC-Pt/CeO_2, b) BC-Pt/CeO_2 and c) AD-Pt/CeO_2. *In situ* DRIFTS of CO adsorption at 30 °C on d) FC-Pt/CeO_2, e) BC-Pt/CeO_2 and f) AD-Pt/CeO_2.

prepared Pt/CeO_2 catalysts, Pt-L_3 EXAFS data were plotted in both K-space and R-space, and curving fitting analysis was also conducted (Fig. 4c-d and Table S3). The exclusive Pt-O coordination shell and the absence of Pt-Pt/Pt-O-Pt coordination shell on AD-Pt/CeO_2 suggested that Pt species were atomically dispersed. In contrast, Pt-O, Pt-Pt and Pt-O-Pt coordination shells were observed on BC-Pt/CeO_2 and FC-Pt/CeO_2, matching well with the results of AC-HAADF-STEM and *in situ* DRIFTS of CO adsorption that agglomerated Pt species were formed on BC-Pt/CeO_2 and FC-Pt/CeO_2. In addition, the relatively lower coordination number (CN) of Pt-Pt and Pt-O-Pt on FC-Pt/CeO_2 ($CN_{Pt\text{-}Pt} = 3.1 \pm 1.3$, $CN_{Pt\text{-}O\text{-}Pt} = 2.1 \pm 1.5$) comparing to AD-Pt/$CeO_2$ ($CN_{Pt\text{-}Pt} = 3.7 \pm 1.7$, $CN_{Pt\text{-}O\text{-}Pt} = 3.4 \pm 1.5$) also supported the observation in AC-HAADF-STEM section that PtO_x clusters on FC-Pt/CeO_2 were much smaller than those on BC-Pt/CeO_2.

For a better illustration of Pt coordination environment, wavelet transform analysis was also applied [49,50], which could provide superior discrimination of atoms with similar coordination conditions and spacings [51]. As shown in Fig. 4e, using PtO_2 and Pt foil as references, it was found that FC-Pt/CeO_2 exhibited three sharp peaks at 2.4, 2.8 and 1.6 Å, corresponding to the first coordination shells of Pt-Pt, Pt-O-Pt and Pt-O, respectively [52]. While for BC-Pt/CeO_2, only two identifiable peaks attributed to Pt-Pt and Pt-O-Pt were observed. In view of the observation that an intensive peak attributed to Pt-O coordination shell (in Pt-O-Ce linkages) on AD-Pt/CeO_2 with the maximum dispersion of Pt, and $CN_{Pt\text{-}O\text{-}Pt}$ for AD-Pt/CeO_2 was higher than that for FC-Pt/CeO_2, it could be concluded that the Pt-O coordination shell observed on FC-Pt/CeO_2 should be mainly related to Pt-O-Ce structure at Pt-CeO_2 interface. That is, more Pt-CeO_2 interfacial sites were formed on FC-Pt/CeO_2 than on BC-Pt/CeO_2. Accordingly, schematic models of the three catalysts were constructed on CeO_2(111) facet for better understanding (Fig. 4**f**).

As previously reported, the local coordination environment of Pt sites on CeO_2 showed a significant impact on their catalytic performance in the catalytic oxidation of various air pollutants (*e.g.*, CO, NH_3 and hydrocarbons, *etc.*). Subsequently, the potential applications of the Pt/CeO_2 catalysts developed in this study will be evaluated using NH3 oxidation, an intensively investigated reaction in the field of environmental catalysis.

3.3. Catalytic performance in NH_3 oxidation reaction

As shown in Fig. 5a, FC-Pt/CeO_2 exhibited significantly higher NH_3 oxidation activity at lower temperatures (150–225 °C) than BC-Pt/CeO_2, suggesting that flattened Pt clusters fabricated by solution combustion method exhibited more superior NH_3 oxidation activity than 3D PtO_x clusters or nanoparticles. In addition, the NH_3 oxidation rate of FC-Pt/CeO_2 (0.154 $\mu mol \bullet g_{cat.}^{-1} \bullet s^{-1}$) is almost twice that of BC-Pt/CeO_2 (0.084 $\mu mol \bullet g_{cat.}^{-1} \bullet s^{-1}$) at 180 °C (Fig. 5b), further confirming the better catalytic performance of FC-Pt/CeO_2. The much lower activation energy (Ea) observed on FC-Pt/CeO_2 also suggested that FC-Pt/CeO_2 could better catalyze the oxidation of NH_3 (Fig. 5c). According to the results of structural characterizations, the higher dispersion of Pt as well as the formation of more oxygen vacancies on FC-Pt/CeO_2 might be the main reasons for the definitive performance advantages of FC-Pt/CeO_2 over

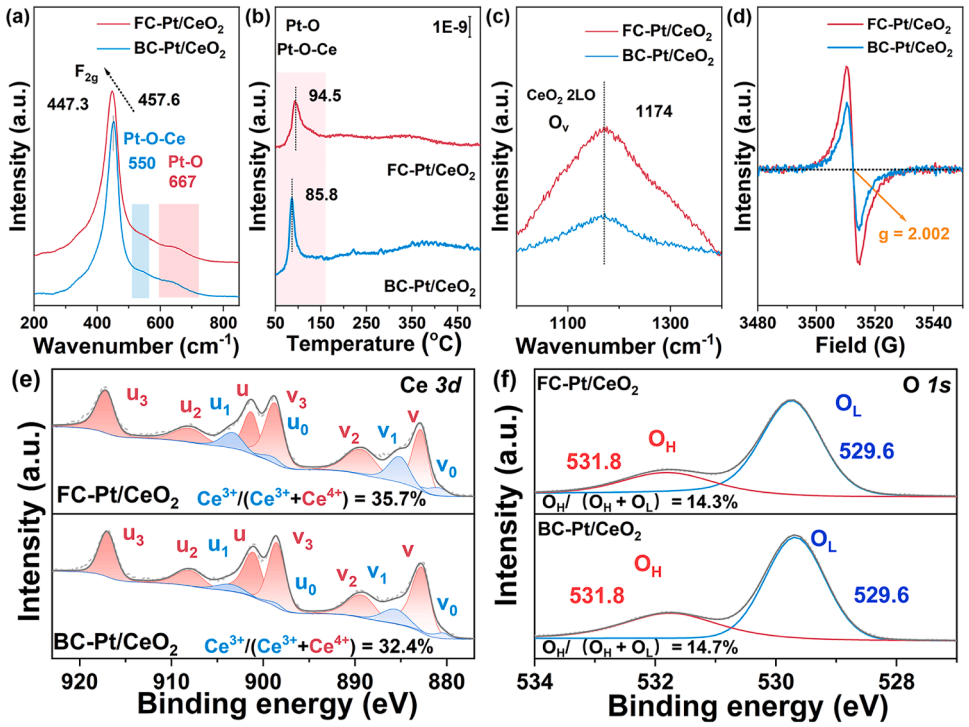

Fig. 3. a) Normalized Raman spectra (200 – 900 cm^{-1}) for FC-Pt/CeO_2 and BC-Pt/CeO_2; b) Full CO-TPR profiles for FC-Pt/CeO_2 and BC-Pt/CeO_2; c) Normalized Raman spectra (1000 – 1400 cm^{-1}) for FC-Pt/CeO_2 and BC-Pt/CeO_2; d) EPR spectra for FC-Pt/CeO_2 and BC-Pt/CeO_2; e) Ce 3d XPS and f) O 1 s XPS for FC-Pt/CeO_2 and BC-Pt/CeO_2.

BC-Pt/CeO_2. Interestingly, although AD-Pt/CeO_2 showed higher Pt dispersion than FC-Pt/CeO_2 and BC-Pt/CeO_2, much inferior catalytic performance was achieved on AD-Pt/CeO_2, highlighting the superiority of the flattened cluster structure. More notably, although FC-Pt/CeO_2 performed the best among the prepared Pt/CeO_2 catalysts, different from the common situation where boosted NH_3 oxidation activity was always at the expense of N_2 selectivity (activity-selectivity trade-off), FC-Pt/CeO_2 still exhibited the highest N_2 selectivity among the prepared Pt/CeO_2 catalysts (Fig. 5d),such discrepancy was mainly due to the reduced formation of non-selective oxidation products including N_2O, NO, NO_2 at high temperatures on FC-Pt/CeO_2 (Figure S8).

Considering that Pt/Al_2O_3 was still the most widely applied catalyst for the selective catalytic oxidation of NH_3 slipped from NH_3-SCR system, in this work, Pt catalyst supported on commercial Al_2O_3 (Pt/Al_2O_3-C) was also prepared as an important reference. Although Pt/Al_2O_3-C and FC-Pt/CeO_2 showed comparable NH_3 oxidation activity, much higher N_2 selectivity was achieved on FC-Pt/CeO_2 (Figure S9). The significant edge in N_2 selectivity enabled FC-Pt/CeO_2 catalyst a promising application prospect. In addition, in order to eliminate the effect of secondary calcination on the specific surface area of the catalysts, we also tested the Pt/CeO_2 catalysts calcined at 500 °C (Figure S10). The FC-Pt/CeO_2 catalysts still showed superior performance enhancement.

Under practical application conditions, the presence of abundant H_2O in the vehicle exhaust might decrease the efficiency of aftertreatment catalyst systems. Taking this into consideration, the catalytic performance of catalysts in the presence of H_2O was also evaluated at 180 °C (Fig. 5e). Although FC-Pt/CeO_2 and Pt/Al_2O_3 showed the same initial NH_3 conversion, after the introduction of H_2O, the decrease in NH_3 conversion on FC-Pt/CeO_2 (from 90 % to 60 %) was much less than that on Pt/Al_2O_3 (from 90 % to 40 %), indicating the better H_2O resistance of FC-Pt/CeO_2. The excellent stability of the FC-Pt/CeO_2 catalyst for NH_3 oxidation reaction was also confirmed by the long-term evaluation at 180 °C (Fig. 5f).

As discussed in the structural characterization section, FC-Pt/CeO_2 and BC-Pt/CeO_2 showed similar capability in O_2 adsorption and activation, which could not explain the exceptional low-temperature activity, H_2O resistance, and prolonged stability observed on FC-Pt/CeO_2. That is, the flattened shape of Pt clusters on FC-Pt/CeO_2 might better facilitate the adsorption/activation of NH_3 and even further alter the reaction pathway, thus improving the catalytic performance.

3.4. *Surface adsorption properties and reaction mechanism*

The NH_3 adsorption characteristics of the prepared Pt/CeO_2 catalysts were first investigated by NH_3-TPD technique (Fig. 6a). Although more weak acid sites (peak α) were formed on BC-Pt/CeO_2 comparing to FC-Pt/CeO_2, the NH_3-TPD profiles for them were quite similar, especially at relatively higher temperatures (> 100 °C, peak β). Considering that the NH_3 oxidation reaction on Pt/CeO_2 catalysts only proceeded above 150 °C, it could be concluded that the amount or the strength of acid sites on BC-Pt/CeO_2 and FC-Pt/CeO_2 were not the main reasons for their distinct catalytic performance in NH_3 oxidation.

To further validate the types of surface acids and quantify their prevalence, pyridine infrared experiments were performed [53]. As shown in Fig. 6b-c, clearly identified adsorption peaks corresponding to Brønsted (B) acid sites (1540, 1620 and 1645 cm^{-1}) and Lewis (L) acid sites (1450, 1580 and 1600 cm^{-1}) [54]. Notably, just as listed in Table 2, the acid sites on BC-Pt/CeO_2 and FC-Pt/CeO_2 were mainly in the form of Lewis acid sites (~75 %). Generally, Lewis acid sites are considered to be crucial for ammonia oxidation reactions due to their ability to activate NH_3 by electron coordination [55,56]. Specifically, Lewis acid sites in the form of metal-oxygen coordination structure can function as active centers by accepting lone-pair electrons from NH_3, followed by the activation of N-H, thus facilitating the further oxidation of NH_3. Since it has been confirmed by NH_3-TPD and *in situ* FTIR spectra of pyridine adsorption experiments that the types (Lewis/Brønsted acid sites) and the strength of acid sites on BC-Pt/CeO_2 and FC-Pt/CeO_2 showed rather limited difference, it was proposed that the detailed coordination environment of Pt sites on BC-Pt/CeO_2 and FC-Pt/CeO_2 should mainly account for the different NH_3 oxidation activity on them.

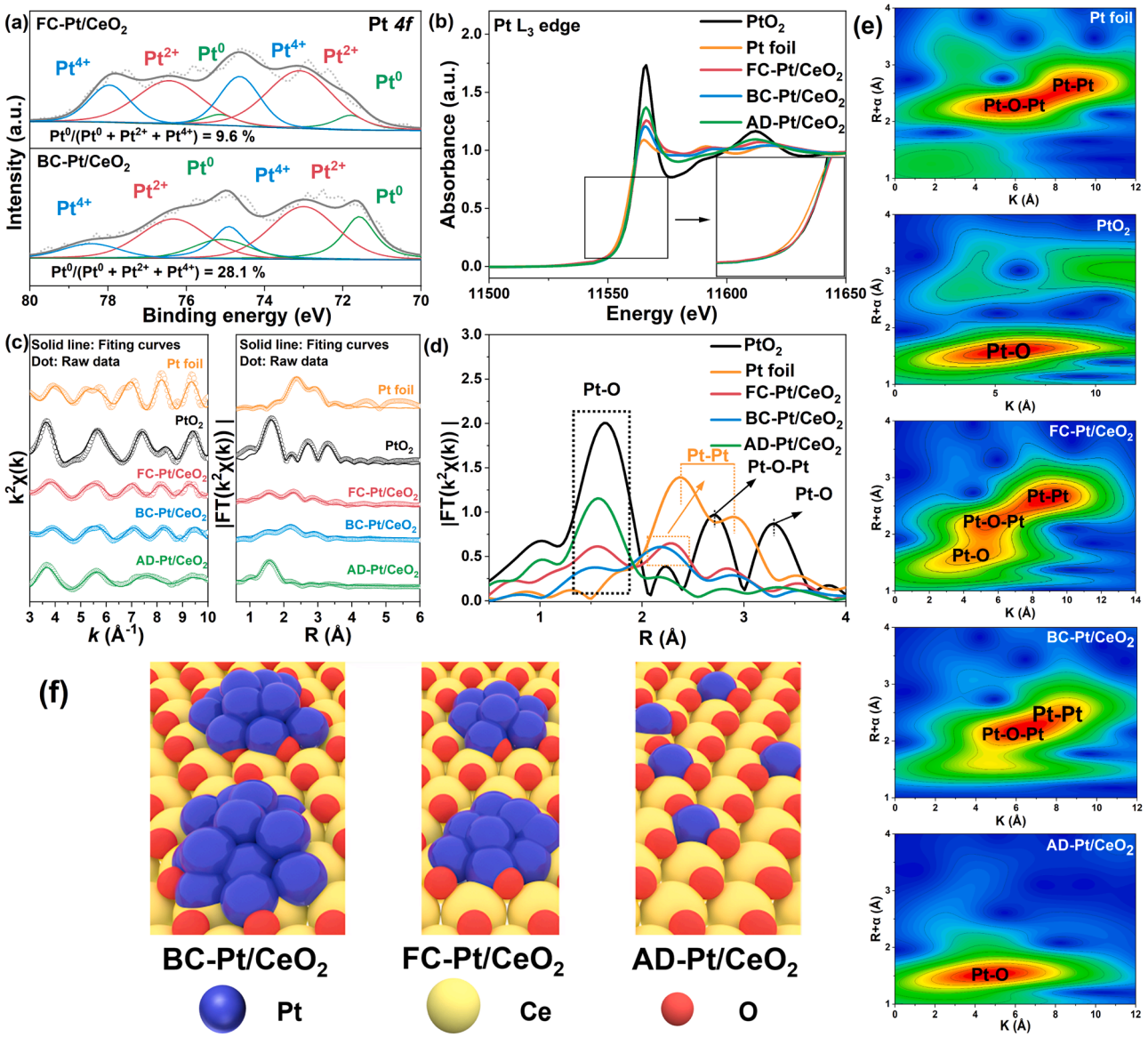

Fig. 4. a) Pt 4 f XPS for FC-Pt/CeO_2 and BC-Pt/CeO_2; b-d) Normalized XANES and EXAFS magnitude of the Fourier transformed k^3-weighted χ(k) data for FC-Pt/CeO_2, BC-Pt/CeO_2 and AD-Pt/CeO_2 at the Pt-L_3 edge. Pt foil and PtO_2 were used as references; e) EXAFS wavelet transform plots of, FC-Pt/CeO_2, BC-Pt/CeO_2 and AD-Pt/CeO_2. f) Schematic structure model for FC-Pt/CeO_2, BC-Pt/CeO_2 and AD-Pt/CeO_2. (Taking the CeO_2 (111) crystal as an example).

To further investigate the relationship between the structure of Pt clusters/particles on and their behavior in NH_3 activation, NH_3+O_2-TPD experiments were performed on FC-Pt/CeO_2 and BC-Pt/CeO_2. The possible generated products (*e.g.*, N_2, NO and N_2O) were monitored by an on-line mass spectrometry. As demonstrated in Fig. 7a-b, N_2 and NO were detected in the outlet gas from FC-Pt/CeO_2 while absent in the outlet gas from BC-Pt/CeO_2 at low temperatures (< 300 °C), and more N_2O was generated on FC-Pt/CeO_2 than on BC-Pt/CeO_2 at lower temperatures (126 °C vs. 143 °C), convincingly proved that NH_3 could be better activated by flattened Pt particles with more Pt-O-Ce interfaces. NH_3-TPSR was also conducted to confirmed the superiority of FC-Pt/CeO_2 in NH_3 activation (Fig. 7c-d). Similar to what was observed in NH_3+O_2-TPD experiment, N_2 and N_2O were generated at much lower temperature on FC-Pt/CeO_2 (148/110 °C) comparing to BC-Pt/CeO_2 (201/132 °C), matching well with our expectation that FC-Pt/CeO_2 could better facilitate the activation and further oxidation of NH_3 than BC-Pt/CeO_2.

To better visualize the surface reaction on Pt/CeO_2 catalysts, *in situ* DRIFTS of O_2 reacting with pre-adsorbed NH_3 experiment under a linear heating condition, *i.e.*, *in situ* DRIFTS of NH_3-TPSR experiment was performed. As shown in Fig. 8a-b and Figure S12, multiple bands corresponding to NH_3 species adsorbed on Lewis acid sites (L-NH_3, 1112 and 1602 cm^{-1}) or Brønsted acid sites (B-NH_3, 1441 cm^{-1}) and -NH_2/-NH groups (1280 and 1420 cm^{-1}) were observed on Pt/CeO_2 catalysts [57]. Besides, IR bands related to nitrate species (1586 cm^{-1}), adsorbed NO (M-NO, 2095 cm^{-1}) [58,59] and adsorbed N_2O (M-N_2O, 2160 cm^{-1}) [60] generated by NH_3 oxidation also emerged. From the standpoint of reaction temperature, it was found that the L-NH_3 species on FC-Pt/CeO_2 could be consumed at lower temperatures comparing to those on BC-Pt/CeO_2, although FC-Pt/CeO_2 and BC-Pt/CeO_2 showed similar *in situ* DRIFTS of NH_3-TPD profiles (Figure S11), which meant that L-NH_3 species on FC-Pt/CeO_2 could be effectively activated and consumed at lower temperatures. Moreover, -NH_2 species derived from L-NH_3 on FC-Pt/CeO_2 also showed better low temperature reactivity to O_2, further confirmed the better capability of flattened Pt clusters in NH_3 activation. Moreover, the simultaneous generation of NO and N_2 on FC-Pt/CeO_2 at 148 °C in NH_3-TPSR experiments (Fig. 7c) and the generation and consumption of adsorbed NO species on FC-Pt/CeO_2 in *in situ* DRIFTS of

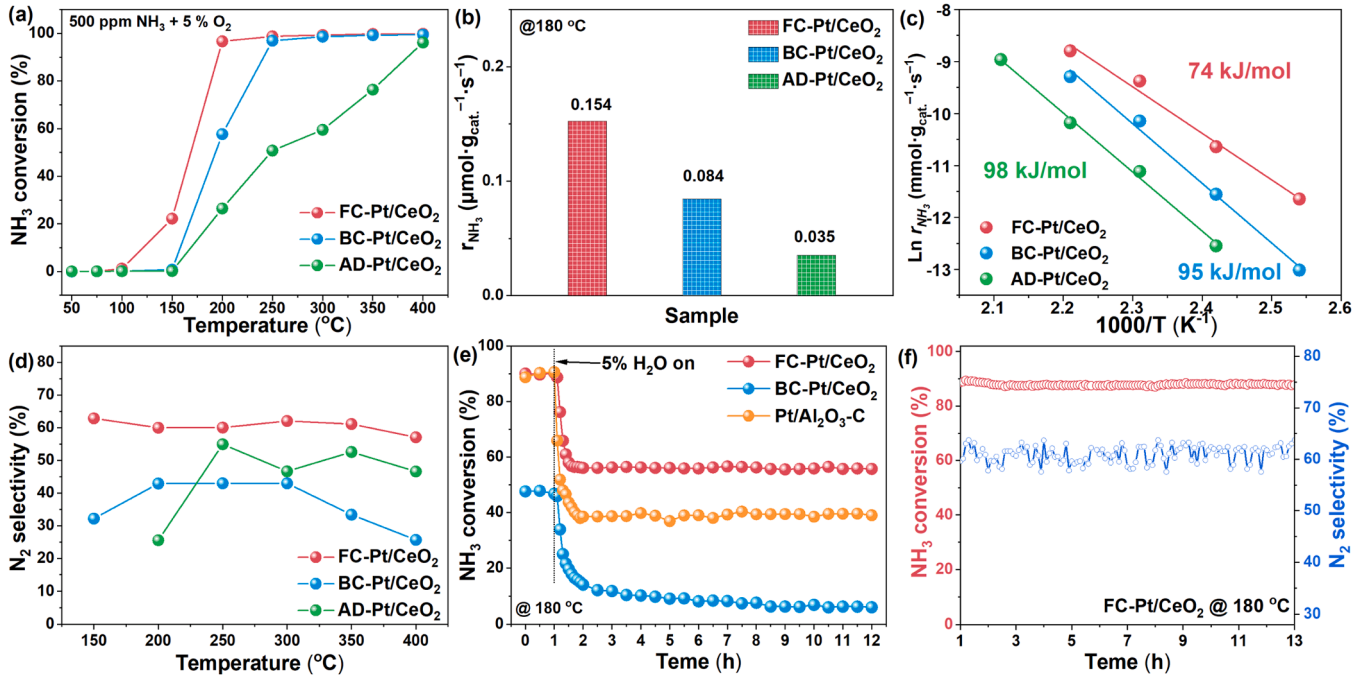

Fig. 5. a) NH_3 oxidation activity for FC-Pt/CeO_2, BC-Pt/CeO_2 and AD-Pt/CeO_2 catalysts; b) the reaction rate of NH_3 oxidation at 180 °C on FC-Pt/CeO_2, BC-Pt/CeO_2 and AD-Pt/CeO_2 catalysts; c) Apparent activation energy of NH_3 oxidation reaction on FC-Pt/CeO_2, BC-Pt/CeO_2 and AD-Pt/CeO_2 catalysts (WHSV = 600,000 mL·$g_{cat.}^{-1}$·h^{-1} for FC-Pt/CeO_2 and BC-Pt/CeO_2 catalysts and 400,000 mL·$g_{cat.}^{-1}$·h^{-1} for AD-Pt/CeO_2 catalyst); d) N_2 selectivity in NH_3 oxidation reaction on FC-Pt/CeO_2, BC-Pt/CeO_2 and AD-Pt/CeO_2 catalysts; e) Effect of H_2O on NH_3 conversion over FC-Pt/CeO_2, BC-Pt/CeO_2 and Pt/Al_2O_3-C catalysts at 180 °C; f) NH_3 oxidation activity on the FC-Pt/CeO_2 catalyst at 180 °C. Reaction condition: 500 ppm NH_3 + 5 % O_2, Ar as balance, WHSV = 100,000 mL·$g_{cat.}^{-1}$·h^{-1}.

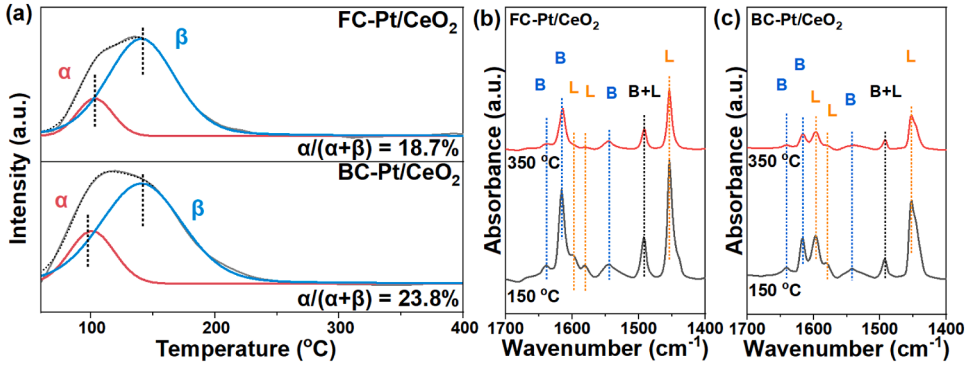

Fig. 6. a) NH_3-TPD profiles for FC-Pt/CeO_2 and BC-Pt/CeO_2; *In situ* FTIR spectra of pyridine adsorption (150 °C and 350 °C) on b) FC-Pt/CeO_2 and c) BC-Pt/CeO_2.

Table 2
NH_3-TPD and Pyridine infrared results for types and densities of surface acids quantified.

Sample	Temperature (°C)	B-acid site area[a]	L-acid site area[b]	L/L+B	Total acid quantity[c]
FC-Pt/CeO_2	150	37.058	125.644	0.772	188.1
	350	18.463	52.297	0.739	
BC-Pt/CeO_2	150	31.235	98.514	0.759	169.7
	350	15.195	43.997	0.743	

[a] Brønsted (B) acid sites =1540 cm^{-1}, 1620 cm^{-1}, 1645 cm^{-1};
[b] Lewis (L) acid sites =1450 cm^{-1}, 1580 cm^{-1}, 1600 cm^{-1};
[c] total acid quantity using NH_3-TPD peak integration results.

NH_3-TPSR suggested that the low-temperature NH_3 oxidation on FC-Pt/CeO_2 could be proceeded by internal SCR (*i*-SCR) reaction pathway [15], through which NO would directly react with NH_3/-NH_2/-NH. The main steps were as followed:

$$\text{-}NH_3 + \text{M-O} \rightarrow \text{-}NH_2 + \text{M-OH} \quad (1)$$

$$\text{-}NH_2 + \text{M-O} \rightarrow \text{M-NH} + \text{M-OH} \quad (2)$$

$$2\text{M-OH} \rightarrow \text{M-O} + \text{M} + H_2O \quad (3)$$

$$O_2 + 2\text{M} \rightarrow 2\text{M-O} \quad (4)$$

$$\text{-NH} + \text{M-O} \rightarrow \text{M-HNO} + \text{M} \quad (5)$$

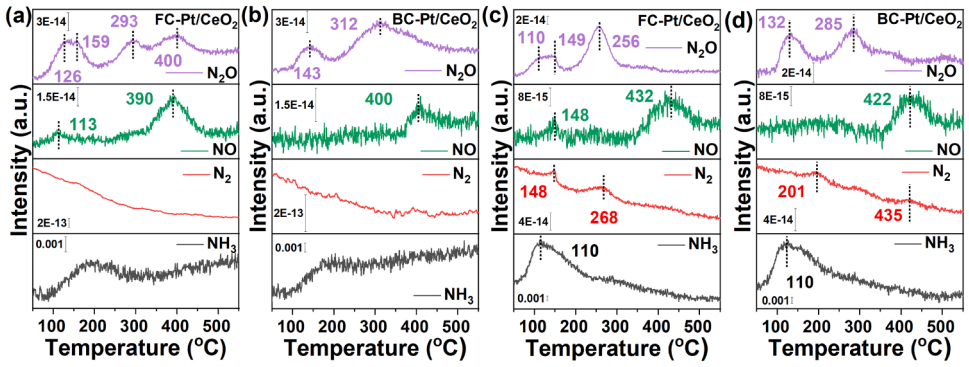

Fig. 7. NH_3+O_2-TPD monitored by mass spectrometry for a) FC-Pt/CeO_2 and b) BC-Pt/CeO_2; NH_3-TPSR monitored by mass spectrometry for c) FC-Pt/CeO_2 and d) BC-Pt/CeO_2.

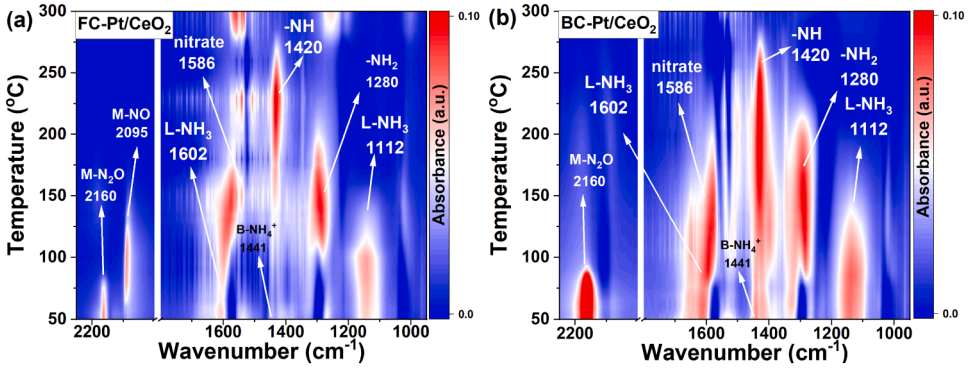

Fig. 8. *In situ* DRIFTS of NH_3 oxidation from 50 °C to 300 °C for a) FC-Pt/CeO_2; b) FC-Pt/CeO_2. Reaction conditions: 500 ppm of NH_3, 1 % O_2 (when used), using Ar or He as balance.

$$M\text{-}HNO + M\text{-}O \rightarrow M\text{-}NO + M\text{-}OH \quad (6)$$

$$M\text{-}NH_2 + M\text{-}NO \rightarrow N_2 + H_2O + 2M \quad (7)$$

$$M\text{-}NH + M\text{-}NO \rightarrow N_2O + \text{-}H \quad (8)$$

$$\text{-}H + M\text{-}O \rightarrow M\text{-}OH \quad (9)$$

where M should be Pt sites.

Specifically, Figure S13 show the *in situ* DRIFTS spectra over FC-Pt/CeO_2 and BC-Pt/CeO_2 catalysts during O_2 injection after NH_3 pre-adsorption. It can be clearly seen that the NH_3 characteristic absorption peaks at 1280 cm^{-1} (corresponding to adsorbed NH_3) and 1112 cm^{-1} (corresponding to linear NH_3) change after oxygen injection. For the FC-Pt/CeO_2 catalyst, the intensity of NH_3 uptake was significantly weakened after the oxygen influx, which suggests that NH_3 is oxidized and converted to other species, indicating a higher efficiency of the oxidation reaction. As for BC-Pt/CeO_2, the absorption peak of NH_3 decayed more slowly, reflecting the effect of different catalyst structures on the reaction path and rate. These data suggest that the FC-Pt/CeO_2 catalyst has stronger Pt-CeO_2 interactions, which may lead to more efficient NH_3 oxidation reactions.

In short summary, the amount, types and strength of the acid sites on FC-Pt/CeO_2 and BC-Pt/CeO_2 were quite similar, however, the flattened Pt clusters with more Pt-O-Ce interfaces and higher oxidation states on FC-Pt/CeO_2 showed clear advantages over 3D Pt clusters on BC-Pt/CeO_2 in NH_3 activation. Due to the efficient activation of NH_3 on flattened Pt clusters, key intermediates (e.g., -NH_2, -NH and -NO), could be generated at lower temperatures, thus contributing to the higher NH_3 oxidation activity on FC-Pt/CeO_2. The interfacial interaction between Pt and the CeO_2 support appears to play a critical role in stabilizing key intermediates and facilitating the complete oxidation pathway.

4. Conclusion

In the field of environmental catalysis, a major concern is how to efficiently catalyze the elimination of pollutants while minimizing the generation of harmful by-products, thereby achieving truly green and environmentally friendly treatments. For NH_3-SCO reaction, it has been widely acknowledged that achieving high catalytic activity and N_2 selectivity simultaneously on a catalyst was not easy, due to the trade-off between low temperature activity and N_2 selectivity, however, in this work, a novel flattened Pt cluster catalyst constructed on CeO_2 support by a solution combustion method was found to exhibit superior catalytic performance in terms of both low temperature activity and N_2 selectivity. The ability of the solution combustion method to synthesize catalysts with high dispersion and strong metal-support interactions provides significant benefits for practical applications in environmental catalysis. Unlike conventional 3D Pt clusters/particles prepared by a commonly used IWI method, flattened Pt clusters with more Pt-O-Ce structure could better facilitate the activation of NH_3 to -NH_2/-NH/-NO at low temperatures, and the efficient reaction between -NH_2 and adsorbed NO via an *i*-SCR reaction pathway enabled satisfactory low-temperature activity and N_2 selectivity on FC-Pt/CeO_2. This work provided new insights into fabricating efficient Pt cluster catalysts with controllable shapes and Pt coordination environment on CeO_2 for environmental catalytic reactions.

CRediT authorship contribution statement

Qinglong Liu: Conceptualization, Data curation, Methodology, Validation, Investigation, Writing. **Jiawei Yang**: Investigation, Data curation, Revision. **Shaoxiong Zhang**: Data curation, Revision. **Song Hong**: Data curation. Hengxiang Zhang: Data curation. **Lupeng Han**:

Revision, Formal analysis. **Dengsong Zhang**: Writing – review & editing. **Fei Gao**: Conceptualization, Formal analysis, Funding acquisition, Project administration, Resources, Supervision. **Wei Tan**: Supervision, Conceptualization, Investigation, Validation, Data curation, Writing – original draft, Writing – review & editing.

Declaration of Competing Interest

The authors declare that they have no known competing financial interests or personal relationships that could have appeared to influence the work reported in this paper.

Acknowledgements

This work was supported by the National Natural Science Foundation of China (Nos. 22372076, 22306090, 22272077), the Natural Science Foundation of Jiangsu Province (BK20230773, BK20231513), Young Elite Scientists Sponsorship Program by CAST (No. YESS20230298), China Postdoctoral Science Foundation (2024M751391, GZB20240304) and Jiangsu Funding Program for Excellent Postdoctoral Talent (2024ZB828).

Appendix A. Supporting information

Supplementary data associated with this article can be found in the online version at doi:10.1016/j.apcatb.2024.124877.

Data availability

Data will be made available on request.

References

[1] R. Verma, M. Singh Sankhla, K. Parihar, R. Kumar, M. Verma, The study of assessing the impact on environment by the noxious airborne chemicals: a review, Biointerface Res. Appl. Chem. 11 (2020) 10844–10863.
[2] R. Nieder, D.K. Benbi, Reactive nitrogen compounds and their influence on human health: an overview, Rev. Environ. Health 37 (2) (2022) 229–246.
[3] M. Liu, X. Huang, Y. Song, J. Tang, J. Cao, X. Zhang, Q. Zhang, S. Wang, T. Xu, L. Kang, X. Cai, H. Zhang, F. Yang, H. Wang, J.Z. Yu, A.K.H. Lau, L. He, X. Huang, L. Duan, A. Ding, L. Xue, J. Gao, B. Liu, T. Zhu, Ammonia emission control in China would mitigate haze pollution and nitrogen deposition, but worsen acid rain, Proc. Natl. Acad. Sci. 116 (16) (2019) 7760–7765.
[4] Y. Huang, S. Liu, M.-M. Pei, J.-Y. Li, H.-D. Xu, Y.-Q. Chen, Unveiling H2O2-optimized NOx adsorption-selective catalytic reduction (AdSCR) performance of WO3/CeZrO2 catalyst, Rare Met. 42 (11) (2023) 3755–3765.
[5] G. He, Z. Lian, Y. Yu, Y. Yang, K. Liu, X. Shi, Z. Yan, W. Shan, H. He, Polymeric vanadyl species determine the low-temperature activity of V-based catalysts for the SCR of NOx with NH3, Sci. Adv. 4 (11) (2018) 4637.
[6] J. Ji, N. Gao, W. Song, Y. Tang, Y. Cai, L. Han, L. Cheng, J. Sun, S. Ma, Y. Chu, C. Tang, L. Dong, Understanding the temperature-dependent H2O promotion effect on SO2 resistance of MnOx-CeO2 catalyst for SCR denitration, Appl. Catal. B Environ. 324 (2023) 122263.
[7] Y. Shan, J. Du, Y. Zhang, W. Shan, X. Shi, Y. Yu, R. Zhang, X. Meng, F.-S. Xiao, H. He, Selective catalytic reduction of NOx with NH3: opportunities and challenges of Cu-based small-pore zeolites, Natl. Sci. Rev. 8 (10) (2021) nwab010.
[8] F. Gao, Y. Liu, Z. Sani, X. Tang, H. Yi, S. Zhao, Q. Yu, Y. Zhou, Advances in selective catalytic oxidation of ammonia (NH3–SCO) to dinitrogen in excess oxygen: a review on typical catalysts, catalytic performances and reaction mechanisms, J. Environ. Chem. Eng. 9 (1) (2021) 104575.
[9] V. Marchuk, D.I. Sharapa, J.-D. Grunwaldt, D.E. Doronkin, Surface states governing the activity and selectivity of pt-based ammonia slip catalysts for selective ammonia oxidation, ACS Catal. 14 (2) (2024) 1107–1120.
[10] C.-Z. Zhu, Q.-H. Tian, B.-H. Wang, M.-T. Xu, Q.-J. Jin, Z.-Y. Zhang, S.-K. Le, Y. Wu, Y.-C. Wei, H.-T. Xu, Application of modified cerium dioxide for photocatalytic air pollution purification, Rare Met. 43 (11) (2024) 5473–5486.
[11] L. Qiao, X. Wang, S. Zong, Z. Huang, Z. Zhou, M. Fan, Y. Yao, Anion-doping-mediated metal–support interactions in CeO2-supported Pd catalysts for CO2 hydrogenation, ACS Catal. 14 (17) (2024) 13181–13194.
[12] H. Yan, H. Lei, X. Qin, J.-C. Liu, L. Cai, S. Hu, Z. Xiao, F. Peng, W.-W. Wang, Z. Jin, X. Yi, A. Zheng, C. Ma, C.-J. Jia, J. Zeng, Facet-dependent diversity of Pt–O coordination for Pt 1 /CeO 2 catalysts achieved by oriented atomic deposition, Angew. Chem. Int. Ed. (2024) e202411264 (n/a, (n/a)).
[13] T. Montini, M. Melchionna, M. Monai, P. Fornasiero, Fundamentals and catalytic applications of CeO2-based materials, Chem. Rev. 116 (10) (2016) 5987–6041.
[14] H. Yan, N. Zhang, D. Wang, Highly efficient CeO2-supported noble-metal catalysts: from single atoms to nanoclusters, Chem. Catal. 2 (7) (2022) 1594–1623.
[15] Y. Cai, X. Ji, B. Zhang, Y. Mu, Q. Tong, A. Liu, W. Tan, F. Liu, L. Dong, Research progress in ceria-based catalysts for the selective catalytic oxidation of NH3. Sci. Sin. Chim. 54 (3) (2024) 295–308.
[16] A. Beniya, S. Higashi, Towards dense single-atom catalysts for future automotive applications, Nat. Catal. 2 (7) (2019) 590–602.
[17] W. Tan, S. Xie, D. Le, W. Diao, M. Wang, K.-B. Low, D. Austin, S. Hong, F. Gao, L. Dong, L. Ma, S.N. Ehrlich, T.S. Rahman, F. Liu, Fine-tuned local coordination environment of Pt single atoms on ceria controls catalytic reactivity, Nat. Commun. 13 (1) (2022) 7070.
[18] C.-Y. Cheng, Y.-Y. Guo, Y.-M. Zou, A.J. Ong, A.I.Y. Tok, S. Li, Melting mechanisms of Pt-based multimetallic spherical nanoparticles by molecular dynamics simulation, Rare Met. 42 (2) (2023) 406–417.
[19] H. Jeong, D. Shin, B.-S. Kim, J. Bae, S. Shin, C. Choe, J.W. Han, H. Lee, Controlling the oxidation state of Pt single atoms for maximizing catalytic activity, Angew. Chem. Int. Ed. 59 (46) (2020) 20691–20696.
[20] C. Ding, Q. Gu, L.-J. Yu, S. Zhang, Y. Zhang, Z. Ma, Y. Meng, H. Zhang, T. Wang, J. Wang, L. Ma, G. Li, B. Yang, T. Zhang, Reversible transformation and distribution determination of diverse Pt single-atom species, J. Am. Chem. Soc. 145 (4) (2023) 2523–2531.
[21] W. Tan, S. Xie, Y. Cai, H. Yu, K. Ye, M. Wang, W. Diao, L. Ma, S.N. Ehrlich, F. Gao, L. Dong, F. Liu, Surface lattice-embedded Pt single-atom catalyst on ceria-zirconia with superior catalytic performance for propane oxidation, Environ. Sci. Technol. 57 (33) (2023) 12501–12512.
[22] F. Dong, Y. Meng, W. Ling, W. Han, W. Han, X. Li, Z. Tang, Single atomic Pt confined into lattice defect sites for low-temperature catalytic oxidation of VOCs, Appl. Catal. B Environ. Energy 346 (2024) 123779.
[23] J. Zhang, X. Qin, X. Chu, M. Chen, X. Chen, J. Chen, H. He, C. Zhang, Tuning Metal–Support Interaction of Pt-CeO2 Catalysts for Enhanced Oxidation Reactivity. Environ. Sci. Technol. 55 (24) (2021) 16687–16698.
[24] E.M. Slavinskaya, A.I. Stadnichenko, J.E. Quinlivan Domínguez, O.A. Stonkus, M. Vorokhta, B. Šmíd, P. Castro-Latorre, A. Bruix, K.M. Neyman, A.I. Boronin, States of Pt/CeO2 catalysts for CO oxidation below room temperature, J. Catal. 421 (2023) 285–299.
[25] H. Wang, J.-X. Liu, L.F. Allard, S. Lee, J. Liu, H. Li, J. Wang, J. Wang, S.H. Oh, W. Li, M. Flytzani-Stephanopoulos, M. Shen, B.R. Goldsmith, M. Yang, Surpassing the single-atom catalytic activity limit through paired Pt-O-Pt ensemble built from isolated Pt1 atoms, Nat. Commun. 10 (1) (2019) 3808.
[26] S. Ge, W. Fan, X. Tang, Y. Cui, D. Wang, X.-Q. Gong, S. Dai, Y. Lou, J. Tang, Y. Guo, W. Zhan, L. Wang, Y. Guo, Revealing the size effect of ceria nanocube-supported platinum nanoparticles in complete propane oxidation, ACS Catal. 14 (4) (2024) 2532–2544.
[27] L.R. Borges, A.H. Braga, D. Zanchet, J.M.R. Gallo, J.M.C. Bueno, CeO2/Pt/Al2O3 catalysts for the WGS reaction: improving understanding of the Pt-O-Ce-Ox interface as an active site, Appl. Catal. B Environ. 325 (2023) 122361.
[28] M. Jabłońska, Progress on noble metal-based catalysts dedicated to the selective catalytic ammonia oxidation into nitrogen and water vapor (NH3-SCO), Molecules 26 (2021) 6461.
[29] S. Cheng, Z. Han, H. Zhao, Y. Li, S. Lu, A novel bifunctional Pt/Ce/WZrOx catalyst for efficient selective oxidation of high-concentration NH3. Chem. Eng. J. 479 (2024) 147876.
[30] T. Lan, Y. Zhao, J. Deng, J. Zhang, L. Shi, D. Zhang, Selective catalytic oxidation of NH3 over noble metal-based catalysts: state of the art and future prospects, Catal. Sci. Technol. 10 (17) (2020) 5792–5810.
[31] Y. Guo, L. Ma, Z. Li, Z. Liu, H. Chang, X. Zhao, N. Yan, Specific reactivity of 4d and 5d transition metals supported over CeO2 for ammonia oxidation, Catal. Sci. Technol. 12 (21) (2022) 6507–6517.
[32] W. Tan, Y. Cai, H. Yu, S. Xie, M. Wang, K. Ye, L. Ma, S.N. Ehrlich, F. Gao, L. Dong, F. Liu, Tuning the Interaction between Platinum Single Atoms and Ceria by Zirconia Doping for Efficient Catalytic Ammonia Oxidation, Environ. Sci. Technol. 57 (41) (2023) 15747–15758.
[33] A.S. Mukasyan, P. Epstein, P. Dinka, Solution combustion synthesis of nanomaterials, Proc. Combust. Inst. 31 (2) (2007) 1789–1795.
[34] E. Carlos, R. Martins, E. Fortunato, R. Branquinho, Solution combustion synthesis: towards a sustainable approach for metal oxides, Chem. – A Eur. J. 26 (42) (2020) 9099–9125.
[35] A. Varma, A.S. Mukasyan, A.S. Rogachev, K.V. Manukyan, Solution combustion synthesis of nanoscale materials, Chem. Rev. 116 (23) (2016) 14493–14586.
[36] C.-T. Yang, B.C. Wood, V.R. Bhethanabotla, B. Joseph, The effect of the morphology of supported subnanometer Pt clusters on the first and key step of CO2 photoreduction, Phys. Chem. Chem. Phys. 17 (38) (2015) 25379–25392.
[37] Y. Xia, J. Ye, D.-g Cheng, F. Chen, X. Zhan, Identification of a flattened Pd–Ce oxide cluster as a highly efficient catalyst for low-temperature CO oxidation. Catal. Sci. Technol. 8 (20) (2018) 5137–5147.
[38] Z. Li, C. Wang, J. Qiu, Y. Ma, C. Wang, X. Sun, K. Li, P. Ning, F. Wang, Advances in selective catalytic oxidation of ammonia (NH3-SCO): a review of catalyst structure-activity relationship and design principles, Chin. Chem. Lett. 35 (1) (2024) 108432.
[39] E. Trusova, N. Trutnev, Cryochemical synthesis of ultrasmall, highly crystalline, nanostructured metal oxides and salts, Beilstein J. Nanotechnol. 9 (2018) 1755–1763.
[40] Z. Jiang, M. Jing, X. Feng, J. Xiong, C. He, M. Douthwaite, L. Zheng, W. Song, J. Liu, Z. Qu, Stabilizing platinum atoms on CeO2 oxygen vacancies by metal-support interaction induced interface distortion: mechanism and application, Appl. Catal. B Environ. 278 (2020) 119304.

[41] X. Liu, X. Ge, J. Cao, Y. Xiao, Y. Wang, W. Zhang, P. Song, W. Xu, Revealing the catalytic kinetics and dynamics of individual Pt atoms at the single-molecule level, Proc. Natl. Acad. Sci. USA 119 (14) (2022) e2114639119.
[42] X.I. Pereira-Hernández, A. DeLaRiva, V. Muravev, D. Kunwar, H. Xiong, B. Sudduth, M. Engelhard, L. Kovarik, E.J.M. Hensen, Y. Wang, A.K. Datye, Tuning Pt-CeO2 interactions by high-temperature vapor-phase synthesis for improved reducibility of lattice oxygen, Nat. Commun. 10 (1) (2019) 1358.
[43] S.-R. Liu, S.-T. Luo, X.-D. Wu, T.-J. Wang, R. Ran, D. Weng, Z.-C. Si, S. Liu, Application of silica-alumina as hydrothermally stable supports for Pt catalysts for acid-assisted soot oxidation, Rare Met. 42 (5) (2023) 1614–1623.
[44] W. Tan, S. Xie, X. Zhang, K. Ye, M. Almousawi, D. Kim, H. Yu, Y. Cai, H. Xi, L. Ma, S.N. Ehrlich, F. Gao, L. Dong, F. Liu, Fine-tuning of Pt dispersion on Al2O3 and understanding the nature of active Pt sites for efficient CO and NH3 oxidation reactions, ACS Appl. Mater. Interfaces 16 (1) (2024) 454–466.
[45] Q. Liu, P. Yang, W. Tan, H. Yu, J. Ji, C. Wu, Y. Cai, S. Xie, F. Liu, S. Hong, K. Ma, F. Gao, L. Dong, Fabricating robust Pt clusters on Sn-doped CeO2 for CO oxidation: a deep insight into support engineering and surface structural evolution, Chem. – A Eur. J. 29 (16) (2023) e202203432.
[46] P. Yang, C. Luo, W. Tan, Q. Liu, S. Zhang, S. Hong, F. Gao, L. Dong, Insights into the construction of robust Pt Clusters with satisfactory stability on CeO2 for the catalytic oxidation of CO, ACS Appl. Mater. Interfaces 16 (17) (2024) 21782–21789.
[47] B. Choudhury, A. Choudhury, Lattice distortion and corresponding changes in optical properties of CeO2 nanoparticles on Nd doping, Curr. Appl. Phys. 13 (1) (2013) 217–223.
[48] C. Schilling, A. Hofmann, C. Hess, M.V. Ganduglia-Pirovano, Raman spectra of polycrystalline CeO2: a density functional theory study, J. Phys. Chem. C 121 (38) (2017) 20834–20849.
[49] H. Funke, A.C. Scheinost, M. Chukalina, Wavelet analysis of extended x-ray absorption fine structure data, Phys. Rev. B 71 (9) (2005) 094110.
[50] H. Funke, M. Chukalina, A.C. Scheinost, A new FEFF-based wavelet for EXAFS data analysis, J. Synchrotron Radiat. 14 (5) (2007) 426–432.
[51] R.O. Savinelli, S.L. Scott, Wavelet transform EXAFS analysis of mono- and dimolybdate model compounds and a Mo/HZSM-5 dehydroaromatization catalyst, Phys. Chem. Chem. Phys. 12 (21) (2010) 5660–5667.
[52] Y. Si, Y. Jiao, M. Wang, S. Xiang, J. Diao, X. Chen, J. Chen, Y. Wang, D. Xiao, X. Wen, N. Wang, D. Ma, H. Liu, Fully exposed Pt clusters for efficient catalysis of multi-step hydrogenation reactions, Nat. Commun. 15 (1) (2024) 4887.
[53] E.P. Parry, An infrared study of pyridine adsorbed on acidic solids. Characterization of surface acidity, J. Catal. 2 (5) (1963) 371–379.
[54] O.M. Busch, W. Brijoux, S. Thomson, F. Schüth, Spatially resolving infrared spectroscopy for parallelized characterization of acid sites of catalysts via pyridine sorption: Possibilities and limitations, J. Catal. 222 (1) (2004) 174–179.
[55] D. Shang, S. Zeng, X. Zhang, X. Zhang, L. Bai, H. Dong, Highly efficient and reversible absorption of NH3 by dual functionalised ionic liquids with protic and Lewis acidic sites, J. Mol. Liq. 312 (2020) 113411.
[56] G. Ramis, L. Yi, G. Busca, M. Turco, E. Kotur, R.J. Willey, Adsorption, Activation, and Oxidation of Ammonia over SCR Catalysts, J. Catal. 157 (2) (1995) 523–535.
[57] C. Wang, Z. Li, X. Sun, Y. Li, L. Shi, S. Zhao, K. Li, P. Ning, F. Wang, Modulating the anchoring states of Ag on TiO2 by SiO2 to boost the NH3-SCO activity over Ag-based catalysts, Appl. Catal. B Environ. Energy 353 (2024) 124091.
[58] T.E. Hoost, K.A. Laframboise, K. Otto, NO adsorption on Cu-ZSM-5: assignment of IR band at 2133 cm−1, Catal. Lett. 33 (1) (1995) 105–116.
[59] Y.H. Yeom, B. Wen, W.M.H. Sachtler, E. Weitz, NOx reduction from diesel emissions over a nontransition metal zeolite catalyst: a mechanistic study using FTIR spectroscopy, J. Phys. Chem. B 108 (17) (2004) 5386–5404.
[60] L. Zhang, H. He, Mechanism of selective catalytic oxidation of ammonia to nitrogen over Ag/Al2O3, J. Catal. 268 (1) (2009) 18–25.